Renewable Energy 107 (2017) 298–311

Contents lists available at ScienceDirect

Renewable Energy

journal homepage: www.elsevier.com/locate/renene

A numerical study on the aerodynamic performance and the self-starting characteristics of a Darrieus wind turbine considering its moment of inertia

A. Arab [a, *], M. Javadi [b], M. Anbarsooz [b], M. Moghiman [a]

[a] Mechanical Engineering Department, Ferdowsi University of Mashhad, Mashhad, Iran
[b] Mechanical Engineering Department, Quchan University of Advanced Technology, Quchan, Iran

ARTICLE INFO

Article history:
Received 22 April 2016
Received in revised form
16 January 2017
Accepted 6 February 2017
Available online 7 February 2017

Keywords:
VAWT
Fluid-solid interaction
Moment of inertia
Darrieus
Transition SST

ABSTRACT

Self-starting characteristics is a challenging issue in the field of Darrieus-type vertical axis wind turbines. Traditionally, the numerical simulations were performed at several constant rotational velocities for the turbine and the generated torques were reported for each rotational velocity, neglecting the effects of the turbine inertia on the transient start-up motion of the turbine. In the current study, a numerical method is proposed to study the self-starting characteristics of a Darrieus wind turbine, considering the turbine moment of inertia. The simulation starts from the initial stationary state and continues until the final steady-periodic condition. At each time step, the instantaneous rotational velocity of the turbine is computed based on the Newton's second law, according to the instantaneous aerodynamic and mechanical forces acting on the turbine. Results indicate that as the rotor inertia increases, it takes a longer time for the turbine to reach its final velocity, in a manner that, the turbine might even fail to reach the final condition and the rotation halts. Results also show that as the rotor inertia decreases, the oscillations amplitude of the turbine rotational velocity increases. This can enable the turbine to pass higher resistant torques than those computed based on the traditional method.

1. Introduction

Being independent of the wind direction and providing a convincing performance in unsteady and skewed wind conditions, have made the Darrieus vertical axis wind turbine an interesting design for researchers especially for urban applications [1]. Although the straight bladed Darrieus turbine is one of the simplest turbines in structure, its aerodynamic behavior is among the most complicated turbines, due to the change in blade angle of attack and Reynolds number during a revolution [2]. In this regard, many researchers have employed various analytical and numerical methods to study different characteristics of Darrieus turbine [1]. What follows is a brief review on these investigations.

Momentum analytical models are the first methods used to study these turbines. Paraschivoiu [3] introduced the double stream-tube analytical model which was more advanced in comparison with the single stream-tube model of Templin [4] and the multiple stream-tube model of Wilson et al. [5]. The analytical momentum theories are suitable for optimization purposes due to their low computational cost [6]. Islam et al. [7] investigated three aerodynamic models, e.g. double-multiple streamtube model, vortex model and the cascade model for performance prediction and design of a straight-bladed Darrieus turbine. The strengths and weaknesses of each model are also discussed. However, these models are only applicable when the employed airfoil data are completely available. Moreover, since these models use the statically determined airfoil data, they lose their accuracy when the airfoil experiences a dynamic stall. These models also suffer from remarkable limits to describe the dynamic effects especially at the turbine startup, where the turbine inertia must be taken into account [8]. These reasons have motivated the computational fluid dynamics (CFD) methods to be adopted widely to study these turbines.

Mohamed [9] studied the aerodynamic performance of an H-rotor Darrieus turbine with 20 different symmetric and non-symmetric airfoils using two-dimensional computational fluid dynamics. Castelli and Benini [10] investigated the effects of the blade inclination angle on the energy absorption efficiency and the

* Corresponding author.
E-mail address: alireza.arab@hotmail.com (A. Arab).

http://dx.doi.org/10.1016/j.renene.2017.02.013
0960-1481/

tangential and axial forces acting on a small Darrieus turbine. Zhang et al. [11] performed numerical investigations on static and dynamic performances of a straight-bladed Darrieus turbine and presented optimized pitch angle along the rotor. Maître et al. [12] studied the main modeling features involved in modeling Darrieus turbines, including the effects of the near-wall grid density and the ability of two-dimensional simulations to represent the actual three-dimensional flow in the turbine. Amet et al. [13] performed a detailed numerical simulation on the blade-vortex interactions in a Darrieus turbine. In contrast to the simulations that consider a constant rotational velocity for the turbine, their study revealed that the flow field around the turbine not only depends on the current flow pattern but also depends on the flow time history [13]. Moreover, since the instantaneous rotational velocity of the turbine depends on the generated torque, and the generated torque is non-uniform in a rotor revolution, the constant rotational velocity assumption for the turbine is an engineering assumption. Therefore, it seems reasonable to employ a numerical method which computes the rotational velocity of the turbine at every time step. Such a numerical method have been recently employed by some researchers to simulate wind turbines.

D'Alessandro et al. [14] and Jaohindy et al. [15] developed a mathematical model considering the interactions between the flow field and the rotor blades for the Savonius drag-based wind turbine. The accuracy of the numerical results were validated by comparison with experimental data. However, no comparison with the traditional methods (which consider a constant rotational velocity for the turbine) have been made. Bazilevs et al. [16] performed full-scale time-dependent aerodynamics and fluid–structure interaction (FSI) simulations of a Darrieus turbine. Their numerical computations demonstrated that the Darrieus turbine might encounter one or multiple dead band regions that the turbine needs to overcome to reach its target rotational speed. Predicting the dead band regions for a Darrieus turbine and computing the necessary external torque to overcome these regions could not be accurately achieved using the traditional methods with constant rotational speed assumption. The effect of the rotor inertia on the turbine startup is another issue that requires a computational methodology where the time dependent fluid structure interactions are taken into account [8,17].

The main aim of the current study is to gain an insight into the complex time-dependent flow field around a Darrieus wind rotor, from its initial staring motion till it reaches its steady target rotational velocity, considering the rotor inertia. In this regard, a CFD based numerical method is developed which considers the fluid-structure interactions in every time step. The instantaneous angular velocity of the rotor, with a single degree of freedom, is determined based on the instantaneous rotor torque. The results obtained using three different turbulence models, k-ω SST, transition SST and k-kl-ω are also compared. Based on the time history of the rotor angular speed, the behavior of the turbine, including its self-starting characteristics, are deliberated in details. The discrepancies between the results obtained from the developed numerical method and those obtained from the traditional methods with constant rotational velocity are discussed. Finally, the effects of the rotor inertia on the startup characteristics of the Darrieus turbine have been investigated.

2. Computational scheme

2.1. Governing equations and turbulence models

Continuity and momentum equations for the two-dimensional turbulent incompressible flow of a Newtonian fluid with constant properties in the differential form are as follows [18,19]:

$$\frac{\partial(\rho\varnothing)}{\partial t} + \mathrm{div}(\rho\varnothing(U - U_g)) = \mathrm{div}(\Gamma_{\varnothing}\mathrm{grad}\varnothing) + S_{\varnothing} \quad (1)$$

$$\varnothing = 1, u, v$$

where ρ is the fluid density, Γ is diffusion coefficient, U is the time-averaged flow velocity vector, U_g is the grid velocity vector and S is the source term.

The appropriate selection of the turbulence model is an essential issue in numerical simulation of the vertical axis wind turbines [20]. Three Unsteady Reynolds Averaged Navier-Stokes (URANS) turbulence models are used in this study which are: the k-ω Shear Stress Transition (SST) model, the k-kl-ω model and the transition SST model. The k-ω SST turbulence model has been successfully employed in various wind turbine simulations [21]. The k-kl-ω model is a three-equation eddy-viscosity type turbulence model which can be used effectively to predict the transition of the laminar boundary layer to turbulent. The three equations are the transport equations for turbulent kinetic energy (k_T), laminar kinetic energy (k_L), and the inverse turbulent time scale (ω). The transition SST model is based on the coupling of the SST transport equations with two other transport equations, one for the intermittency and one for the transition onset criteria, in terms of momentum-thickness Reynolds number [22]. Details of the employed turbulence models are available in Refs. [22–24].

The CFD commercial software, Ansys Fluent 15.0, is used to solve the time-dependent governing equations. The diffusion and convention terms are discretized using the second order linear upwind scheme. Pressure-momentum equations coupling is performed using the PISO (Pressure-Implicit with Splitting of Operators) algorithm [22].

The torque coefficient, C_m, power coefficient, C_p, and the tip speed ratio, TSR, are determined using the following relations [25–27]:

$$C_m = T/\tfrac{1}{2}\rho RAV_{\infty}^2 \quad (2)$$

$$TSR = \omega R/V_{\infty} \quad (3)$$

$$C_p = C_m \times TSR \quad (4)$$

where R is the turbine radius, A is the turbine frontal area, V_∞ is the air velocity, ω is the rotor angular velocity and T is the torque.

2.2. Computational domain and grid

The computational domain is divided into two regions, a rotating circular region around the rotor blades and a rectangular stationary region, as shown in Fig. 1. The two regions are connected using an interface boundary condition, where the continuity of the absolute velocity is imposed to provide the correct neighbor velocity values for the rotating subdomain [22]. A structured O-grid of quadrilateral elements is generated around the rotor blades to ensure the necessary grid resolution on walls. At a distance of two times the blade chord away from the blades, an unstructured grid is generated as depicted in Fig. 2, while an unstructured triangular grid is used for the rest of the computational domain.

2.3. Mathematical model of the rigid body motion

The employed computational strategy consists of three main components: flow solver, a six-degree-of-freedom (6-DOF) motion solver and a sliding mesh algorithm. At each time step, first, the

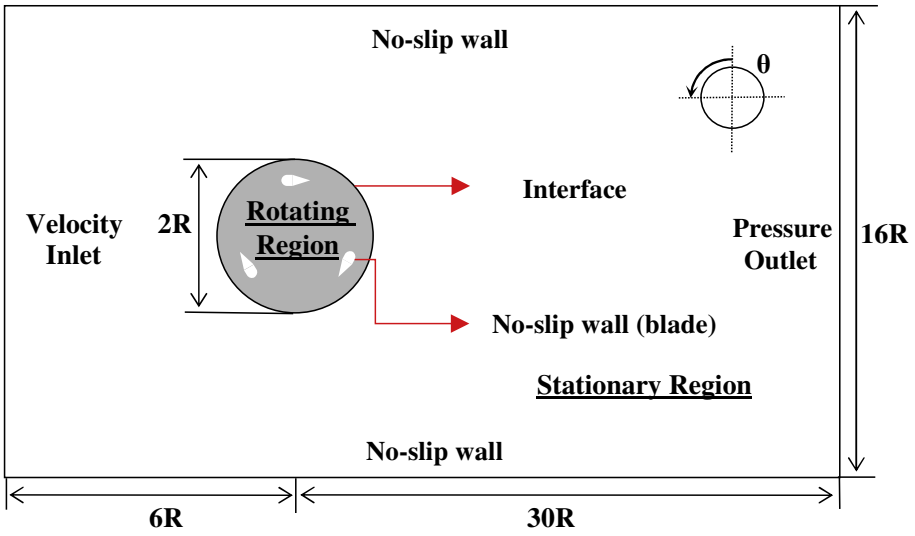

Fig. 1. Computational domain and boundary conditions.

fluid flow governing equations (which are the Reynolds-Averaged-Navier-Stokes equations) are solved using the Fluent flow solver. From the resulting solution, the aerodynamic moment acting on the rotor are determined. Next, the motion solver uses the aerodynamic moment and the external torques to calculate the rotational movement of the rotor. Finally, the sliding mesh algorithm, rigidly rotates the rotor subdomain (rotating region) to its position for the next time step.

The details of the RANS solver are available in Fluent Theory Guide and hence, they are not repeated here. However, some explanations are warranted about the formulation of governing equations on a moving computational domain. Eq. (1) in the integral from for a general scalar quantity, φ, on a moving domain can be written as [28]:

$$\frac{\partial}{\partial t}\int_V \rho\varphi dV + \int_{\partial V} \rho\varphi(U - U_g).d\vec{A} = \int_{\partial V} \Gamma\nabla\varphi.d\vec{A} + \int_v S_\varphi dV \qquad (5)$$

The time derivative in the expression above is evaluated using a first-order backward difference formula:

$$\frac{d}{dt}\int_V \rho\varphi dV = \frac{(\rho\varphi V)^{K+1} + (\rho\varphi V)^K}{\Delta t} \qquad (6)$$

where the superscript denotes the time level. V^{k+1} in (6) is

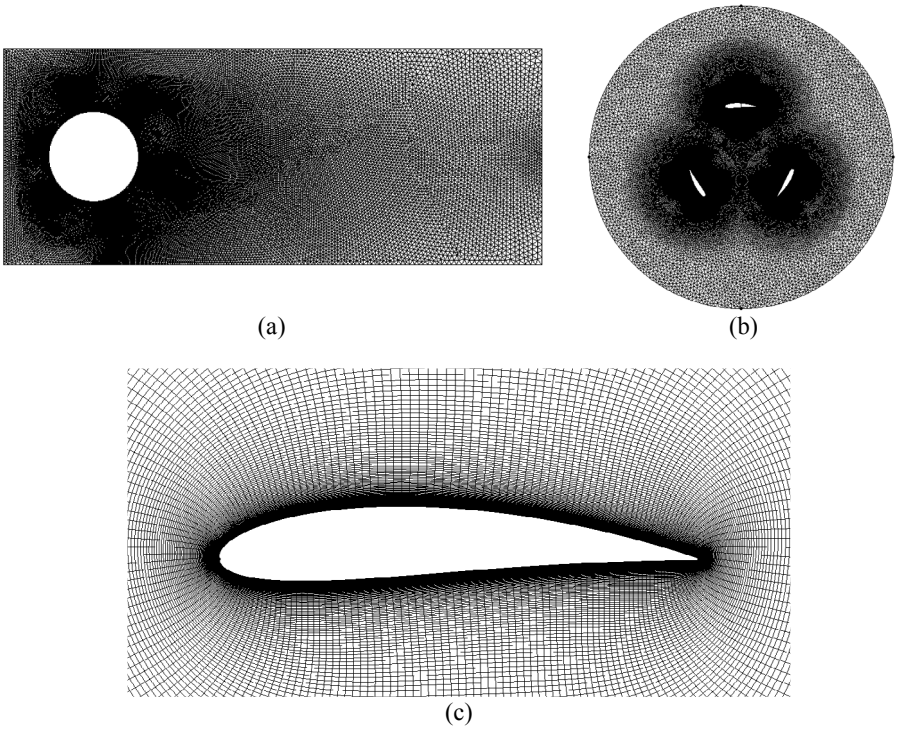

Fig. 2. The grid distribution inside the computational domain, a) the stationary zone, b) the rotating zone, and c) mesh resolution around the rotor blade.

evaluated as:

$$V^{k+1} = V^k + \frac{dV}{dt}\Delta t \tag{7}$$

Because the mesh motion in the sliding mesh formulation is rigid, all cells retain their original shape. As a result, the time rate of change of the cell volume is zero.

$$V^{k+1} = V^k \tag{8}$$

As a result, Eq. (6) can be written as:

$$\frac{d}{dt}\int_V \rho\varphi dV = \frac{\left((\rho\varphi)^{K+1} + (\rho\varphi)^K\right)V}{\Delta t} \tag{9}$$

First, At every time step, the fluid flow governing equations are solved using the Fluent commercial software. Knowing the flow field variables, the aerodynamic moments acting on the rotor blades can be determined by integrating the pressure and viscous forces over the blades, as:

$$M_p = \sum_f \left[r_f \times \left(p_f a_f\right)\right] \tag{10}$$

$$M_\tau = -\sum_f \left[r_f \times \left(\tau_f a_f\right)\right] \tag{11}$$

where M_p and M_τ are the resultant torques of the pressure and viscous forces exerted on the blades by the wind, p_f is the pressure and τ_f is the shear stress, a_f is the area vector of the face f, and r_f is the distance vector from the body center of mass to the center of face f. The summation is performed on all of the computational cells on the rotor blades. Then, the total moment acting on the turbine, M, is determined as follows:

$$M = M_p + M_\tau + M_r \tag{12}$$

where, M_r is any external resistant torques on the rotor such as the generator load.

Next, these moments are transferred to the 6-DOF code which has been written in C language and dynamically linked with the Fluent solver at run time. Its aim is to calculate the rotor rotational speed at each time step based on its rotational speed at the previous time step and the torque which is exerted on the rotor by the wind. In this study, the rotor has only one degree of freedom which is rotating around the turbine axis and the other 5° of freedom are constrained. This calculation is performed using the Euler's law of motion, as:

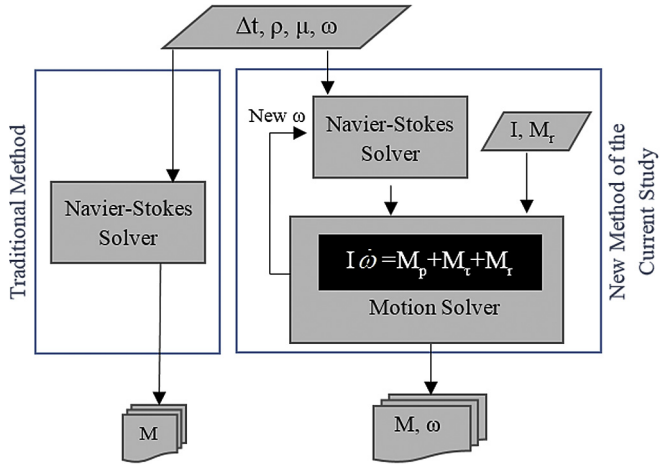

Fig. 3. Flowchart of the solution process in comparison with the traditional schemes.

Table 1
Geometrical parameters of the computational domain.

Parameter	Value	Parameter	Value
Airfoil type	NACA4515	Chord length	0.1 m
Domain width	5 m	Turbine radius	0.3 m
Domain length	10 m	Inner region radius	0.9 m

$$\dot{\vec{\omega}} = I^{-1}\left(\sum \vec{M} - \vec{\omega} \times I\vec{\omega}\right) \tag{13}$$

where $\dot{\vec{\omega}}$ is the rotor rotational acceleration vector, $\vec{\omega}$ is the rotor angular velocity vector and I is the rotor inertia tensor. Once the angular acceleration is computed from the above equation, the rotor angular velocity at the next time step is determined using a fourth-order multi-point Adams-Moulton formulation [28], as:

$$\vec{\omega}^{k+1} = \vec{\omega}^k + \frac{\Delta t}{24}\left(9\dot{\vec{\omega}}^{k+1} + 19\dot{\vec{\omega}}^k - 5\dot{\vec{\omega}}^{k-1} + \dot{\vec{\omega}}^{k-2}\right) \tag{14}$$

where k is the time-step counter.

When the rotor angular velocity at the new time step is known, the sliding mesh method is used to rigidly rotate the grids of the rotating zone to their new position. In the sliding mesh method, the coupling between the rotating and stationary zones are performed using the non-conformal mesh-interface treatment available in the Fluent software [29–31].

Fig. 3 shows the flowchart of the solution process in comparison with the traditional scheme [12]. In the traditional scheme, the rotational velocity of the rotor is assumed constant and the solution of the Navier-Stokes equations leads to the corresponding output torque of the turbine. This process will be performed for several constant rotational velocities to produce the C_m-TSR curve for the turbine. By contrast, in the new method of the current study, the solution starts with an initial rotor rotational velocity and the corresponding torque is determined through the solution of the Navier-Stokes equations. Then, the new rotational velocity for the next time step would be calculated by applying the equations of motion, where the rotor inertia and the turbine resistant torque are also required as the inputs. Next, the solution of the Navier-Stokes equations will be repeated using the new rotational velocity. This cycle will be repeated until the steady-periodic condition is achieved.

Table 2
The main characteristics sizes of the three grid resolutions, used for the grid-study.

	Coarse	Medium	Fine
Number of cells on the blade	100	200	400
Non-dimensional height of the first cell on the blade (Y^+)	10	1.2	0.53
Diameter of the area with structured grid	3 times the chord length	3 times the chord length	3 times the chord length
Number of cells on the interface	70	120	250
Number of cells on the outer boundary	20	40	100

3. Verification and validation

For the verification investigations, the dimensions of the computational domain and the boundary conditions are selected according to the experimental conditions of Takao et al. [32] at the air velocity of 7 *m/s*. The main geometrical parameters of the turbine and the computational domain are presented in Table 1.

In order to achieve grid-independent results, three grid resolutions namely, the coarse, medium and fine grids have been examined. The main characteristic sizes of these grids are given in Table 2. The variations of the torque coefficient for one blade as a function of the angular position of the rotor is shown in Fig. 4, for the three grid resolutions at TSR = 1.6. As the figure suggests, the medium grid can be selected as the best grid, in terms of both the numerical accuracy and computational cost.

The effects of the domain extents on the output torque are also examined. The goal is to place the boundaries at a sufficient distance to avoid any influence on the evaluation of the flow field around the turbine. In this regard, 6 different cases are tested at TSR = 1.0 and the results are presented in Table 3. Three rotor distances from the inlet boundary (1R, 6R and 20R) and three rotor distances from the outlet boundary (10R, 30R and 90R) are investigated. The results show that Case B, where the rotor distances from the inlet and outlet boundaries are 6R and 30R, respectively, can be selected as the best size for the computational domain. Further increasing the size of the computational domain does not have significant effects on the generated torque.

In order to investigate the time step effects on the transient numerical results, three time steps have been considered, as given in Table 4. Since in this study, the initial transient motion of the turbine has also been considered, the rotational velocity of the turbine is not constant and varies with time. Therefore, it seems more appropriate to apply the time step in terms of a portion of the blade revolution. In this regard, the UDF capability of the Ansys Fluent software has been used to adjust the time step in a manner that it would produce a constant value for the rotor revolution in every time step [22].

Table 4
The time steps considered for simulations.

Blade revolution in one time-step (degrees)	0.125	0.25	1
Time step (milliseconds)	0.0571	0.1142	0.4568
Number of time steps required for one revolution	2880	1440	360

The computations time, required for the smallest time step of Table 4, is eight times longer than that of the largest one, which indicates the importance of selecting an appropriate time step. Fig. 5 shows the effects of the time step on the torque coefficient of one blade at the average TSR = 1.6. As the figure illustrates, the time step which corresponds to 0.25° of revolution, is the most suitable one, since it satisfies both the accuracy and computational cost criteria.

In order to validate the numerical results, the averaged values of the power coefficient as a function of the TSR are compared with the experimental data of Takao et al. [32]. For the numerical simulations, three turbulence models have been employed, k-ω SST, transition SST and k-kl-ω. Fig. 6 shows the numerical results of torque coefficient as a function of the TSR, in comparison with those of experiments. As the figure shows, the numerical results obtained using the Transition SST turbulence model are in a better agreement with the experimental data. Therefore, this turbulence model has been adopted for all of the following numerical investigations.

4. Results and discussion

As stated before, the main goal of the current study is to investigate the aerodynamic characteristics of the transient start-up process of the Darrius wind turbine. As shown in Fig. 6, the working range of the studied rotor is up to TSR≈2.5. In order to better illustrate and interpret the transient results, for all the following results, the simulations are performed with a rotor radius of 1.0 *m* (all the other geometrical parameters of the turbine are

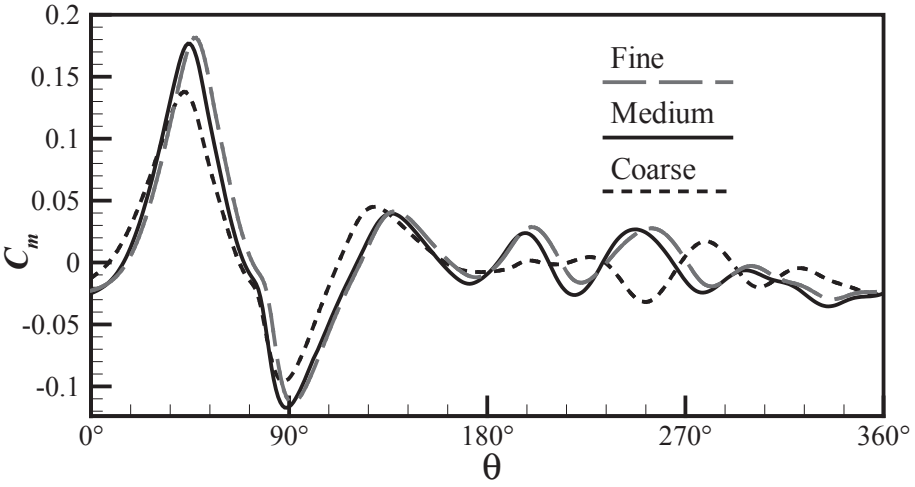

Fig. 4. The variations of the torque coefficient for one blade, as a function of the rotor angular position, for the three grid resolutions at TSR = 1.0.

Table 3
The effects of the computational domain extends on the torque coefficient at TSR = 1.

	A	B	C	D	F	G
Distance from the inlet boundary	1R	6R	20R	6R	6R	20R
Distance from the outlet boundary	30R	30R	30R	10R	90R	90R
C_m	0.0728	0.054	0.0532	0.0894	0.0564	0.0562

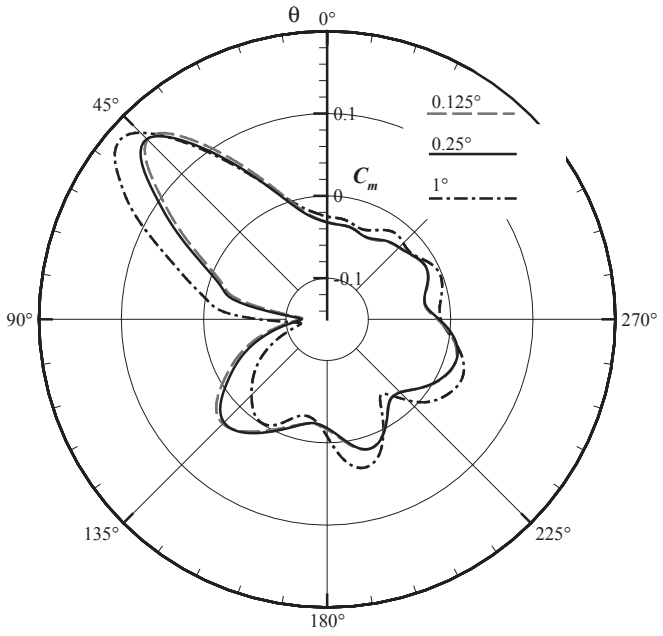

Fig. 5. Time step effects on the torque coefficient of one blade, in one revolution.

kept constant). Increasing the rotor radius, decreases the turbine rigidity and as a result, it would extend the working range of the turbine [33]. The effect of increasing the rotor radius on the torque coefficient is shown in Fig. 7. As the figure shows, the working range of the turbine has been extended up to TSR ≈ 5.3.

Fig. 8 shows the time variations of the rotor TSR, for three various incident wind speeds and two dimensionless rotor inertias. The dimensionless rotor inertia, I^*, is defined as the ratio of the turbine inertia to the inertia of an air cylinder with a same radius as that of the turbine:

$$I^* = \frac{I_{turbine}}{\frac{1}{2}M_{air}R^2} = \frac{I_{turbine}}{\frac{1}{2}(\rho_{air}\pi R^2 H)R^2} \tag{15}$$

The rotor starts rotating from its zero initial velocity and accelerates until it reaches its final steady-periodic condition, where the rotor rotational velocity oscillates around a mean value. As the figure shows, increasing the wind speed from 7 *m/s*, to 15 and 25 *m/s*, has shortened the required time for the rotor to reach its steady-periodic state. Moreover, such an increase in the wind speed, has increased the mean final TSR, which is 10 and 15% for the wind speeds of 15 and 25 *m/s*, respectively. An interesting feature of this figure is that, unlike the previous studies, even at the final steady-state condition, the rotor oscillates around a mean value. The frequency of these oscillations, also increases with increasing the wind speed. In other words, the wind speed or the flow Reynolds number has considerable effects on the required time of the turbine to reach its final steady condition and also on the average and the frequency of oscillations of the final TSR. Fig. 8 demonstrates that, even at the final condition, the rotor rotational velocity oscillates around a mean value. In order to refer to such an oscillatory rotational velocity, the rotor dimensionless rotational velocity, TSR, is modified to ATSR (Average Tip Speed Ratio), as given below:

$$\text{ATSR} = \overline{\omega}R/U_\infty \tag{16}$$

where $\overline{\omega}$ is the average rotational velocity of the rotor at the final steady-periodic condition.

The effects of the rotor average rotational velocity on the generated torque of one blade in a full rotor revolution is depicted in Fig. 9, at four ATSRs. As the figure shows, the rotor rotational velocity has significant effects on the generated torque of the blade, however, the effect is different on the upstream ($0° < \theta < 180°$) and downstream sides ($180° < \theta < 360°$). For the upstream side, as the rotor rotational velocity increases, the peak torque coefficient also increases, marginally. Furthermore, the oscillations of the C_m for $80° < \theta < 360°$ vanishes as the wind speed grows. For the downstream side, at ATSR = 0.5, there are several fluctuations with a negative average value. Nevertheless, as the ATSR increases up to 3.0, the fluctuations of C_m decrease and its average value increases. At ATSR>3.0, the fluctuations are weak and the average C_m tends to zero.

Weak starting characteristics is one of the main drawbacks of the Darrieus-type vertical axis wind turbines [34,35]. In other words, these turbines are generally unable to reliably self-start, due to a critical region of weak or even negative torque, especially at low TSRs. In some azimuthal angles in a complete rotor revolution, the direction of the resultant aerodynamic forces acting on the blades are opposite the direction of rotor rotation. In a certain rotational speed, if the average of these forces in a rotor revolution is negative, it is said that the rotor is in the negative average torque status. Negative average torque means that the rotor could not

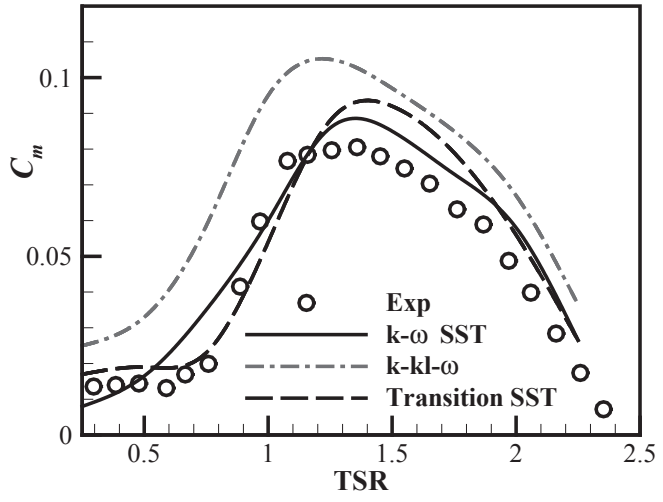

Fig. 6. The numerical results comparison with the experimental data of Takao et al. [23], using various turbulence models.

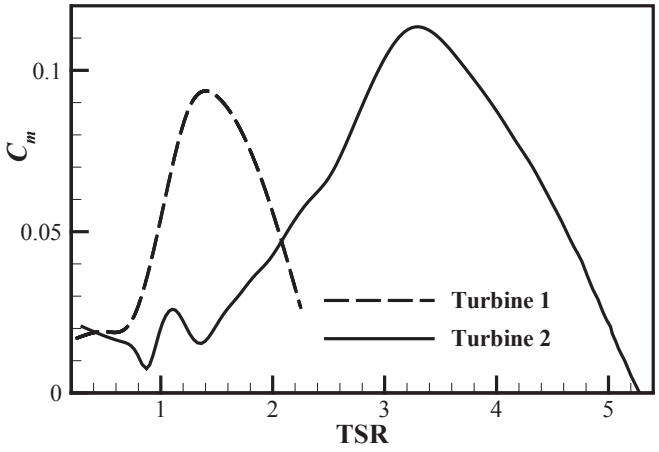

Fig. 7. The effect of increasing the rotor radius on the torque coefficient of the turbine.

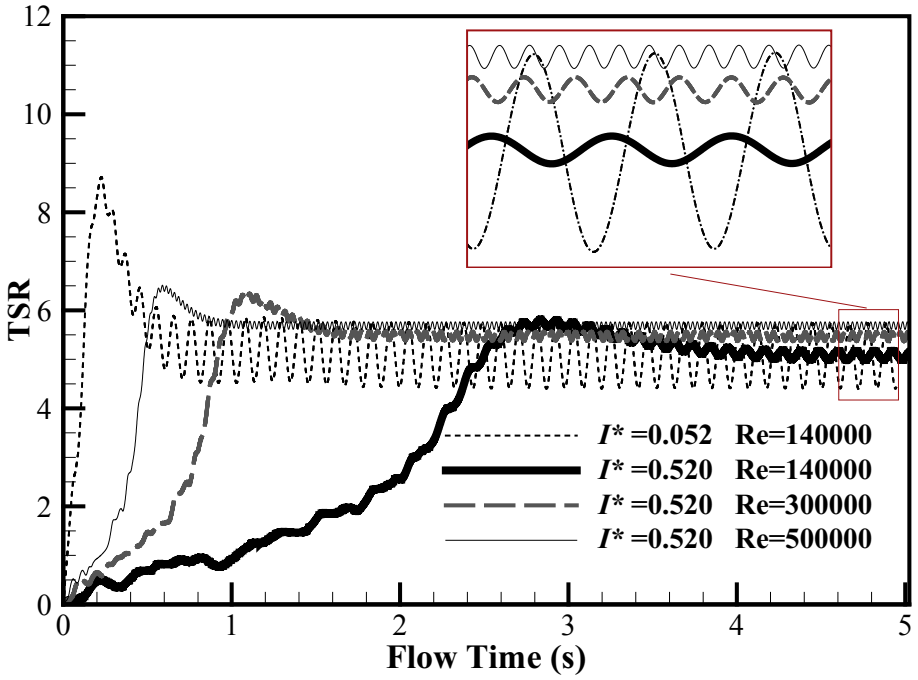

Fig. 8. Time variations of the rotor TSR, for three various incident wind speeds and two dimensionless rotor inertias.

overcome the drag forces and it needs an external force to be able to keep its rotational speed, otherwise, the rotor angular speed will decrease. In other words, the generated lift forces cannot overcome the resisting drag forces and the rotor needs an external force such as a starter motor to pass that rotational speed.

The main reason of negative torque is the drag force which is a resisting force. At all of the angular speeds, at least in a portion of the rotor revolution the drag force overcomes the lift force, and causes an instantaneous negative torque. The main trouble is when the drag negative torque overcomes the lift positive torque in a complete rotor revolution and the average torque becomes negative. At this circumstance, the turbine angular velocity will not increase. Typically, this status occurs for the Darrieus turbine at low angular velocities (TSR≈1.0). That is because at low angular velocities, the amplitude of the blades angle of attack is great and as a result, large angle of attacks occur. At these conditions, especially after the stall point, the blade lift coefficient decreases considerably, while the drag coefficient increases.

Despite the previous methods [12], which consider a constant velocity for the turbine, the proposed method in this study is able to determine the transient acceleration of the turbine, from the initial condition up to the final steady condition, continuously. Referring

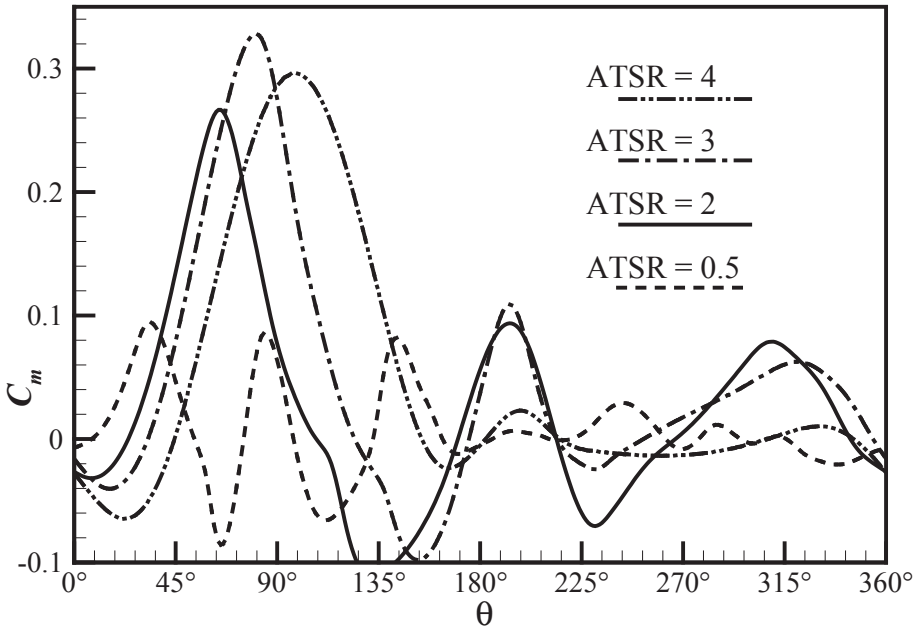

Fig. 9. Torque coefficient as a function of the rotor angular position at various ATSRs.

to Fig. 11, the turbine accelerating process can be separated into three stages: I) Starting from the stationary condition up to TSR = 1.0, where the turbine passes its critical region, II) speeding up from TSR = 1.0 up to TSR = 4.0, and III) the final stage, where the acceleration decreases until it reaches its final steady-periodic condition.

Before investigating the first stage, it seems beneficial to study the initial condition of the turbine which might affect the start-up process of the turbine. In other words, the initial values of the flow field, used in the numerical simulations, might have considerable effects on the required time to reach the final steady condition and also on the reliability of the results. In this regard, four initial conditions have been considered for the numerical simulations, which are the results of: a) a steady solution for a stationary rotor, b) an unsteady solution for a stationary rotor, until the steady-state condition is achieved, c) a solution performed using the sliding mesh method assuming a constant rotational velocity for the rotor at TSR = 0.2, until the steady-state condition is achieved and d) a solution strategy similar to (c) but at TSR = 1.0. These four conditions are representatives of various initial conditions that might occur in the experimental measurements.

Fig. 10 shows the initial distributions of the vorticity around the rotor blades for the four mentioned initial conditions. As the figure shows, there are several vortices around the blades, except for case (a). The effects of these initial conditions on the start-up process of the turbine is depicted in Fig. 11. Case (a) has a noticeably higher starting acceleration in comparison with the three other cases, which is mainly due to the non-existence of the vortices at the initial condition. However, all the four cases have converged to a same final steady-periodic condition, despite their different paths to reach the final state. This figure shows that the existence of the initial vortices would lead to a slower starting of the turbine, which is mainly because of the lower lift forces of the blades. The worst case in this figure is case (c), which has reached the final state even later than the case (a). The vortices in case (c) has indeed affected

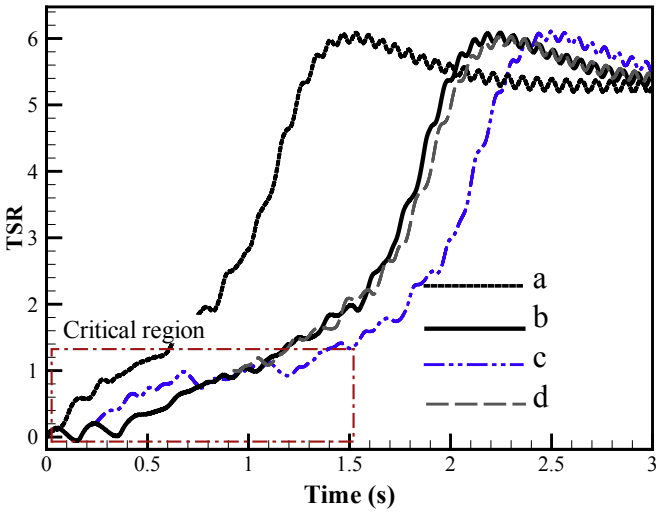

Fig. 11. The effects of the initial conditions on the turbine start-up process.

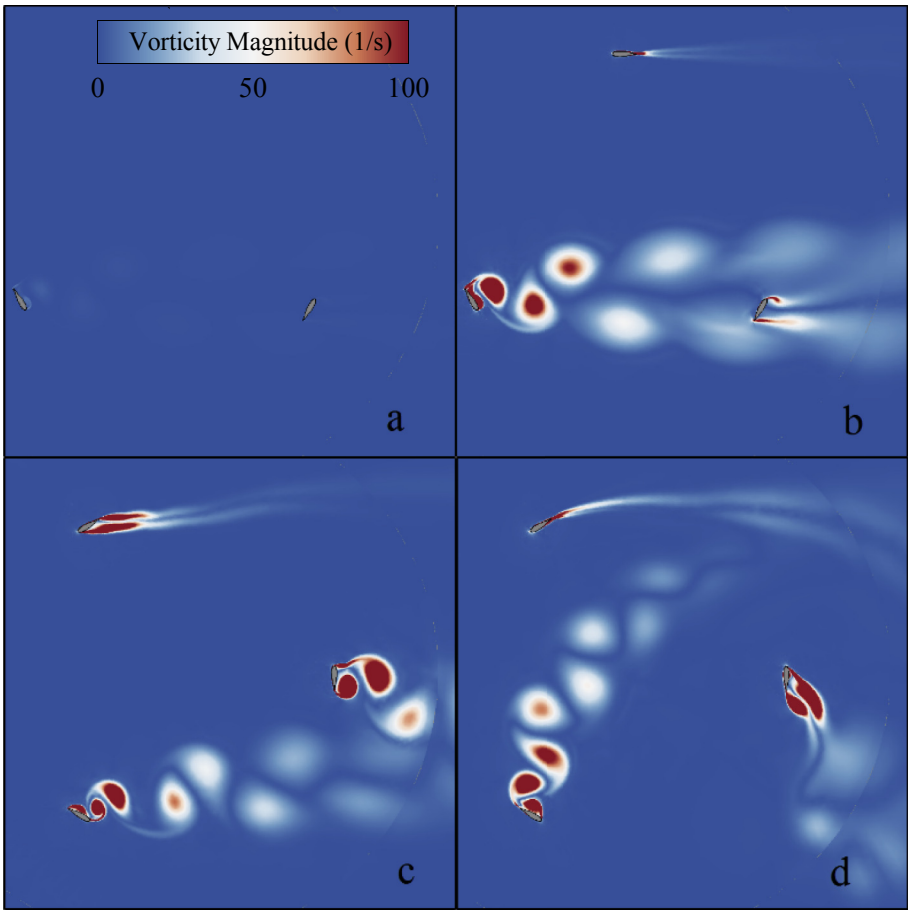

Fig. 10. Vorticity distributions around the rotor blades for several initial conditions.

the aerodynamic performance of the turbine in a manner that it has reached the final state even later than the rotor which has started its motion from the stationary state.

Despite the previous methods such as the sliding mesh methods with the assumption of a constant rotational velocity for the turbine, in the proposed numerical scheme developed in the current study, the effects of the history of the flow field could be investigated on the transient start-up process of the turbine. Nevertheless, as can be seen in Fig. 11, the effects of the initial condition is only considerable up to TSR ≈ 1.0; after that, all the curves have almost equal accelerations.

In order to explain the reason of the low starting acceleration at the first stage (TSR<1.0), the variations of the blade geometrical angle of attack in first half of revolution are plotted in Fig. 12 as a function of the rotor angle for several TSRs. In this figure, the geometrical angle of attack has been plotted considering the relative wind velocity. Hence, the blade geometrical angle of attack is a function of both the rotor angle and also the TSR, as given in Eq. (11) [3]:

$$\alpha = \tan^{-1}\left(\frac{\sin\theta}{\cos\theta + \mathrm{TSR}}\right) \tag{17}$$

It must be noted that the geometrical angle of attack is slightly different with the effective angle of attack, experienced by the blade. It is due to the induced wind velocity which has been caused by the wake and body. However, both angles follow a same trend and especially for the first half of rotation, the difference is negligible. Thus, the geometrical angle of attack is good enough for addressing the various observed phenomenon of the studied Darrieus turbine.

As the figure shows, at TSR = 1.0, the geometrical angle of attack oscillates between 0 and 90°. The airfoil of the current study, NACA4415, would stall for the angle of attacks larger than about 15° [36]. Therefore, the blade will produce positive lift only in a small range of the rotor angles (approximately θ < 30°), and for the rest of the rotor angles, the blade would stall or even produce negative lift. This, is the reason for the weak starting torque of the turbine for 0 < TSR<1.0. However, as the TSR increases, the range in which the blade produces positive lift extends and consequently, for TSR>1.0, the generated torque and the rotor acceleration increase.

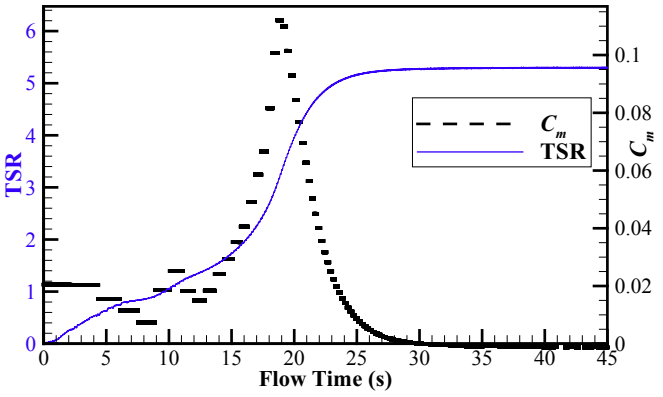

Fig. 13. Time variations of the torque coefficient and the TSR.

Fig. 13 shows the time variations of both the TSR and the torque coefficient. The values of the torque coefficients have been averaged in one revolution of the turbine, which are plotted with dashed lines. Each separate dashed line is the averaged torque coefficient in one turbine revolution. Thus, the width of each line indicates the period of one revolution and the number of lines shows the number of turbine revolutions. As the figure shows, in contrast to the drag-based turbines, the starting torque of this turbine is weak. It increases as the turbine TSR increase, until it reaches its maximum value and then decreases marginally to zero. Since no external torque has been applied to the turbine, the turbine TSR would increase until the torque coefficient becomes zero.

As can be seen in Fig. 13, there is a minimum in the torque coefficient at 0 < TSR<1.0. In order to justify this behavior, it must be noted that both the drag and lift forces produce the output torque of the turbine. However, the drag force is only available up to TSR = 1.0, where the blade speed would be equal to the wind speed and as a result, there would be no drag force. Furthermore, as discussed above, at TSR<1.0 the lift force is weak, due to the large angles of attack. Therefore, at TSR<1.0, the main driving force of the turbine is the drag force, which is also minimum at TSR = 1.0. This result, suggests that in order to enhance the ability of the turbine to pass its critical region, the turbine output torque at TSR = 1.0 has to

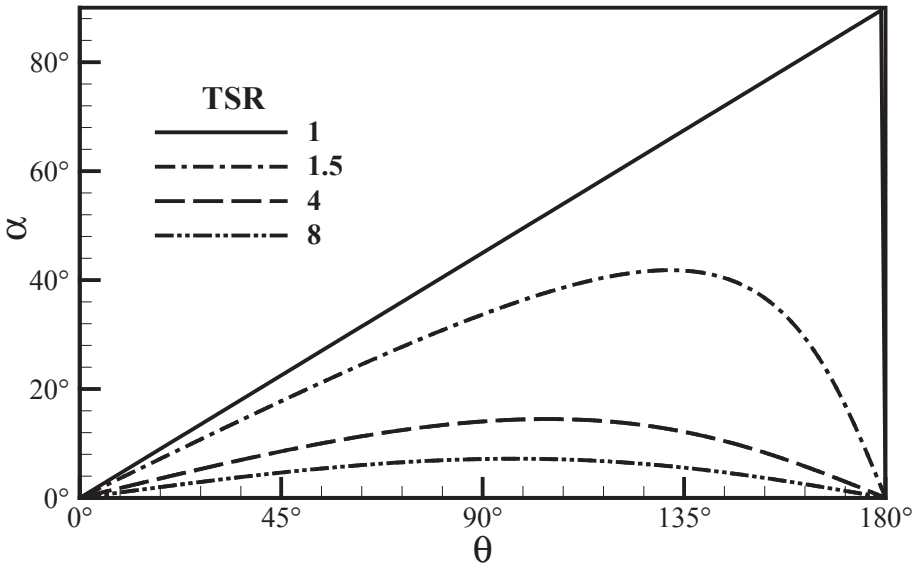

Fig. 12. Blade geometrical angle of attack, α (deg), as a function of the rotor angle, θ (deg), for several TSRs.

be enhanced. Hence, not only the blade lift coefficient, but also its drag coefficient at the critical region is essential. Zamani et al. [37,38] employed the J-Shaped profile for the blade airfoil which improved the drag force at the start-up of the turbine. Previous studies also indicate that the higher thickness airfoils, ensuring a higher drag coefficient, have provided superior self-starting characteristics [33,39]. It might be concluded at the current conditions, employing the Savonius rotors (with a maximum torque coefficient at TSR≈1.0) to improve the self-starting characteristics of the Darrieus turbine, can be more efficient in comparison with the bucket-type drag-based turbines (with a maximum torque coefficient at TSR≈2/3). Furthermore, in order to take advantage of thick airfoils at the critical region and at the same time, avoid their drawbacks at higher TSRs, asymmetric airfoils, could be employed. The selected asymmetric airfoil must have a higher drag coefficient in comparison with the symmetric airfoils at high TSRs, and a lower drag coefficient at low TSRs, in comparison with the thick airfoils.

After passing its critical stage (0 < TSR<1.0), the turbine enters the second stage, which is named here, *the acceleration stage*, (1.0 < TSR<4.0). As discussed above, as the TSR increases above 1.0, the range in which the blade produces positive lift extends and as a result, the generated torque and the rotor acceleration increase.

Fig. 14 demonstrates the vorticity contours around the rotor blades, at various instants of rotor acceleration. As the time passes, the rotor TSR increases. At each instant, the values of the torque coefficients are also depicted on the figures. The low initial torque and its increasing rate as the TSR grows above 1.0, can also be explained using this figure.

First, at low TSRs such as TSR = 1.0, while the wind passes the width of the turbine, the blade would sweep the volume of the air only once. As a result, a considerable amount of the wind energy would pass the turbine, without losing its exergy. However, as the rotational velocity of the turbine increases to TSR = 4.0, the front blade would sweep the air 4 times and this would capture a higher amount of the wind energy. Second, as the collected energy by the upstream blade increases, a lower amount of the wind energy would reach the downstream blade, where the negative torque would be generated. And third, as the TSR increases, the maximum angle of attack that the blade experiences in one revolution would be lower than the stall angle of attack. The resultant unseparated flow, would increase the lift and hence, the turbine efficiency. For example, at TSR = 4.0, the maximum geometrical angle of attack in one revolution is 14.5° which is lower than the blade stall angle (the static stall angle for the current blade is 15°, which might slightly differ from its dynamic stall angle).

The third stage, *the final stage*, occurs at TSR>4.0, where the increasing rate of the turbine rotational velocity decreases, until it reaches the final steady-periodic condition. The high rotational velocity of the blades, increases the pressure at the front of the turbine and the turbine acts as a rigid cylinder that a large portion of the wind passes around it (see Fig. 14). This is called the blockage effect which reduces the blades lift forces and the turbine efficiency. Moreover, at high TSRs such as TSR = 5.3, the geometrical angle of attack would oscillate between −10° and +10°. Although no separation would occur, the low angles of attack decreases the maximum possible lift force of the blades. Moreover, at high TSRs, the blades drag force would increase, which dominates the lift-driven torque of the turbine and as a result, the turbine acceleration tends to zero. As can be clearly seen in Fig. 14, the vortices detached from the upstream blade and collides the downstream blade at TSR = 1.0, are significantly different from those at TSR = 4.0. It is also possible that the vortices detached from the upstream blade at TSR = 1.0, reach the downstream blade at a higher TSR. As shown before, these vortices might have considerable effects on the transient start-up motion of the turbine. Therefore, in contrast to other turbo-machineries, considering the flow history is essential for investigating the critical state of these turbines.

The effects of the turbine moment of inertia on its final steady-periodic condition, are demonstrated in Fig. 15. The external resistant torque coefficient, C_{Mr}, is also determined using the following relations:

$$C_{Mr} = \frac{M_r}{\frac{1}{2}\rho RAV_\infty^2} \tag{18}$$

In this figure, the angular variations of the rotor TSR is plotted for two external resistant torque coefficients of C_{Mr} = 0.028 and 0.094, for three rotor inertias of I^* = 0.051, 0.26 and 0.51.

The results of the traditional method, assuming a constant rotational velocity for the turbine, are also depicted in this figure. In the traditional method, the rotor moment of inertia and also the external torque, have no effects on the simulation results, since these parameters have not been taken into account in the governing equations. However, the results of the proposed method in this study, show that as the rotor moment of inertia increases, the amplitude of the rotor oscillations decreases. Maitre et al. [12] compared their numerical results for the torque coefficient in a rotor revolution with their experimental data. The comparison showed a phase shift between the numerical and experimental data, however, no justification has been presented. The results of the current study reveals that, the phase shift is due to the rotor inertia, which hasn't been considered in their numerical simulations.

Not only the moment of inertia, but also the external torque affects the amplitude of the rotor oscillations, as shown in Fig. 16. In this figure, the generated torque of one blade and its TSR are plotted as a function of the rotor angular position, in a full rotor revolution, in comparison with the traditional method. This figure shows that the velocity oscillations and the generated torque interact with each other. When the blade reaches the turbine front, at $\theta = \pi/2$, it produces the maximum torque. This is why the angular variation of the turbine TSR, shown in Fig. 15, has three maximums in one revolution; the turbine has three blades and each blade when reaches the turbine front, generates a maximum in the TSR-θ graph. The generated torque is a function of the blade lift force which itself is a function of the blade velocity. In the traditional method, the rotor angular velocity is constant and as a result, the generated torque at arch rotational velocity is also constant. In the proposed method of this study, the rotor angular velocity at the final steady-periodic condition, oscillated about a mean value. At $\theta \sim 75°$, the rotor angular velocity is less than its averaged angular velocity (based on the traditional method) and therefore, the generated torque is less than that of the traditional method, as can be seen in Fig. 15. Similarly, as the rotor angular velocity increases and gets larger than the average value, the generated torques of the current method are also higher than those of the traditional method. The generated torque is a function of the blade lift force, which itself is a function of the blade velocity. At $\theta \sim 75°$ the blade relative velocity is less than its average velocity and as a result, the computed torque is less than the prediction of the traditional method. As the blade speed increases, at $\theta \sim 110°$, the lift force and the generated torque have increased. Similarly, at $\theta \sim 210°$, the blade drag force has increased and caused more negative torque. This figure reveals that considering a constant rotational velocity for the turbine might overestimate or underestimate the generated torque of the turbine. The proposed method of the current study does not suffer from this drawback.

The variations of the turbine instantaneous power coefficient as a function of the rotor TSR is plotted is Fig. 17 at the final steady-

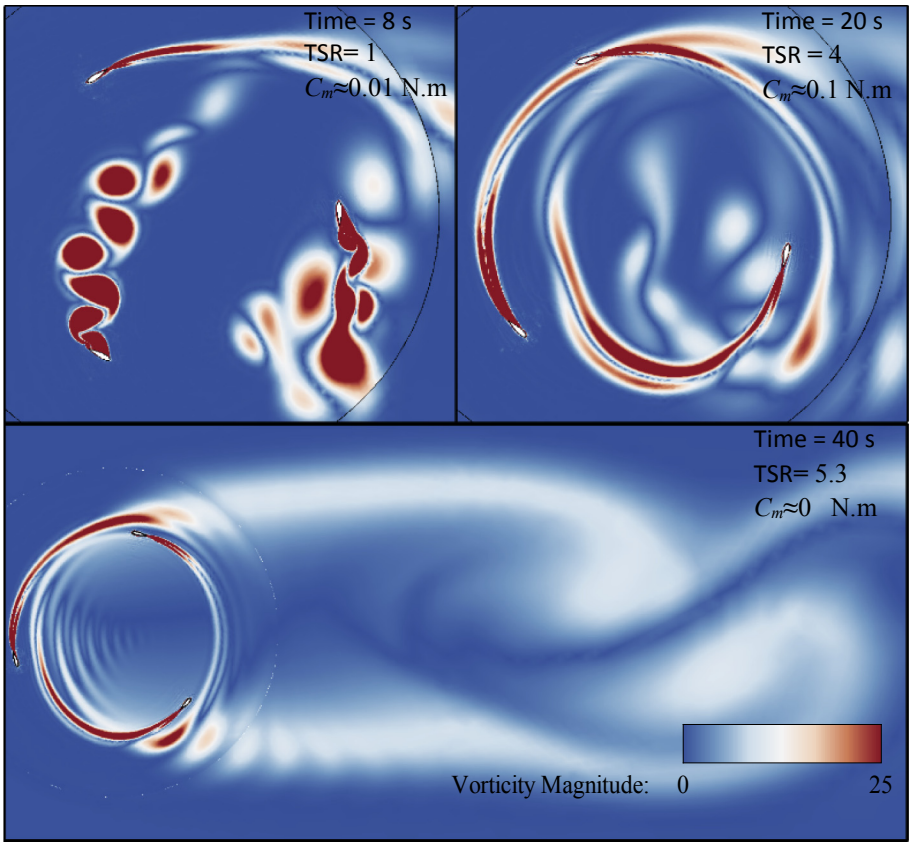

Fig. 14. Vorticity contours around the rotor blades, at various instants of rotor acceleration.

periodic condition, for two external resistant torque coefficients of C_{Mr} = 0 and 0.094, for three dimensionless rotor inertias of I^* = 0.051, 0.26 and 0.51. The figure demonstrates that considering the turbine moment of inertia and also the external resistant torque, affects the amplitude of the power coefficient oscillations. For the turbine investigated in this study, as the turbine moment of inertia decreases, the discrepancy between the results of the current method and the traditional method increases. In the other words, the oscillations of the rotors with low moment of inertias are relatively high, and therefore, the assumption of constant rotational velocity is not appropriate for these rotors.

The oscillations of the torque coefficient, especially for the rotors with low moment of inertias, would affect the accuracy of the critical resistant torque of the turbine. As shown in Fig. 7, the C_m-

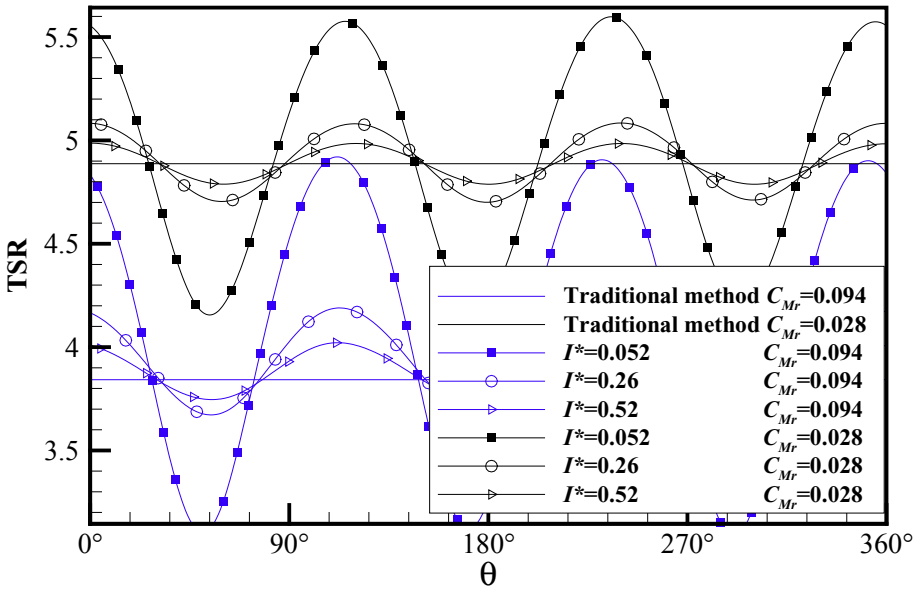

Fig. 15. The angular variations of the rotor TSR for various dimensionless rotor inertias and external torques.

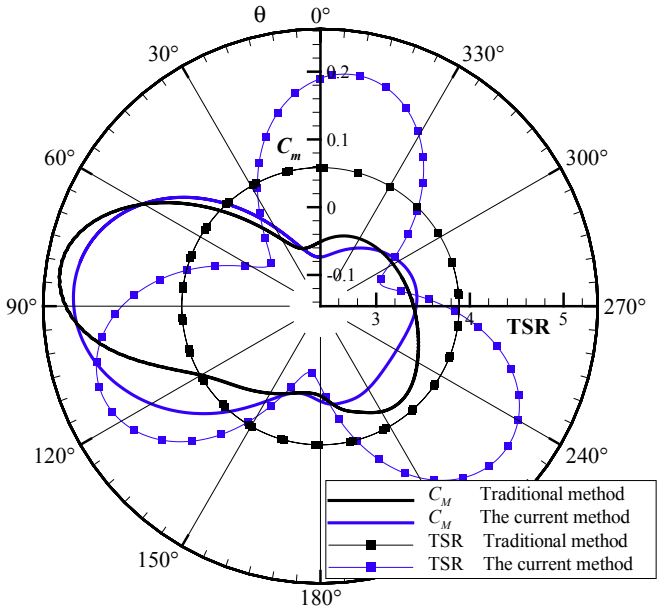

Fig. 16. Comparing the results of the current method for the torque coefficient variations as a function of the TSR, with those of the traditional method.

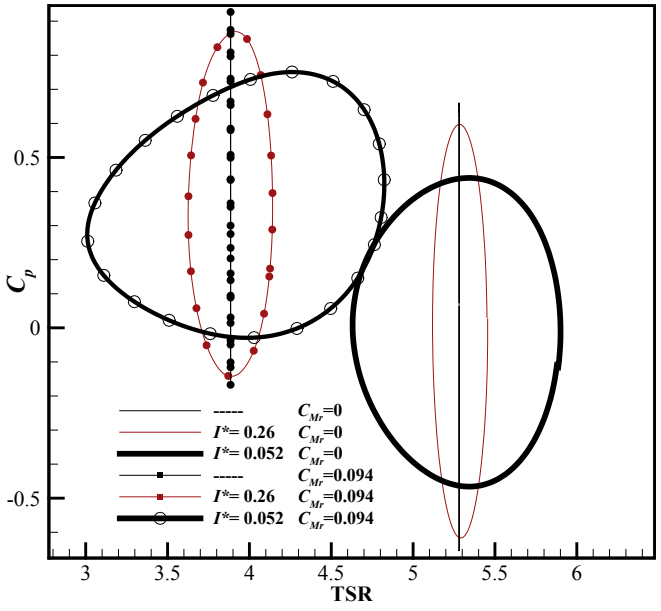

Fig. 17. The variations of the turbine instantaneous power coefficient as a function of the rotor TSR at the final steady-periodic condition, for several external resistant torques and rotor inertias.

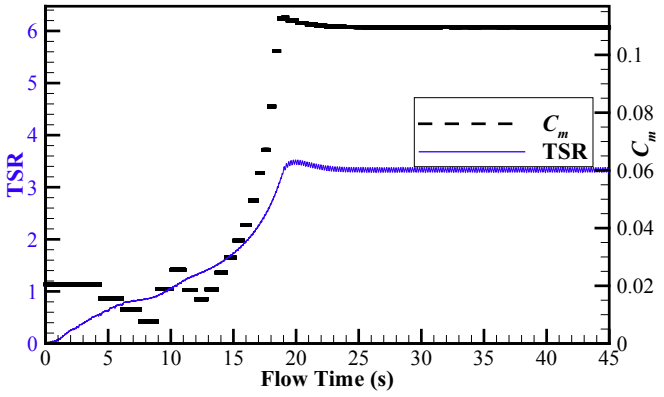

Fig. 18. Time variations of the rotor TSR and torque coefficient, when the turbine is subjected to a resistant torque of $C_{Mr} = 0.11$.

TSR curve for the turbine under study, has a minimum at TSR ≈ 0.9. If the external torque of the turbine, exceeds this critical value, the turbine wouldn't reach its final steady-periodic condition. Based on the traditional method calculations, the critical value of the torque coefficient for the present turbine is 0.079, neglecting the rotor inertia. However, the results obtained using the method proposed in this study for the required time for the turbine to reach its final state are presented in Table 5, for various values of the external resistant torque coefficient, C_{Mr}, and several values for the dimensionless rotor moment of inertias, I^*. In this table, 'Failed' means that the rotor has failed to reach its final steady condition. As can be seen in the table, the rotors with the dimensionless moment of inertias greater than 2.598, exposed to a resistant torque coefficient of $C_{Mr} = 0.08$, have failed to reach their final steady state condition, as correctly been predicted by the traditional method. However, for the rotor with the smallest dimensionless moment of inertia ($I^* = 0.053$), the turbine has succeeded to pass its critical stage and it has reached the final steady rotational velocity of the rotor, as explained before. This table clarifies that the results of the traditional method are not satisfactory for the wind rotors with small moment of inertias. Thus, the proposed method of the current study can be effectively employed by the researchers to determine when they can neglect the turbine moment of inertia and when they cannot.

The developed numerical method is also capable of applying a resistant torque to the turbine at any given time. In this regard, a resistant torque equal to the maximum available torque is applied to the turbine, when it has reached the corresponding rotational speed. The transient acceleration of the turbine and also the torque coefficient are illustrated in Fig. 18. The applied resistant torque coefficient is $C_{Mr} = 0.11$. As can be seen in the figure, when the external torque is applied, the turbine stops accelerating and rotates at a constant rotational velocity.

Table 5
The required time (in seconds) for the turbine to reach its final steady periodic condition, as a function of the dimensionless turbine moment of inertia, I^*, and the external resistant torque coefficient, C_{Mr}. In this table, 'Failed' means that the rotor couldn't reach the final steady condition.

I^*	c_{Mr}								
	0	−0.013	−0.040	−0.066	−0.080	−0.093	−0.107	−0.120	−0.133
0.052	0.5	0.5	0.6	0.7	1	1.1	2	2.1	Failed
0.520	4.2	4.5	6.3	10.5	19	43	Failed	Failed	Failed
1.039	8	8.4	12	43.2	112	Failed	Failed	Failed	Failed
2.598	17	20.2	31	126	198.4	Failed	Failed	Failed	Failed
5.197	30	33.4	37.3	89.6	359	Failed	Failed	Failed	Failed
26.984	145	150.3	155.4	247	Failed	Failed	Failed	Failed	Failed

5. Conclusions

In this study, a numerical method is proposed to study the effects of the turbine moment of inertia and external resistant torques on the self-starting characteristics of a Darrieus wind turbine, based on the unsteady solution of the Navier-Stokes equations. The simulations initiate from the stationary state and continue until the final steady-periodic condition. According to the instantaneous aerodynamic and mechanical forces acting on the turbine, the rotational velocity at each time step is computed based on the Newton's second law. The main findings of the current study can be summarized as below:

- Investigating several initial conditions revealed that, the aerodynamic performance of the turbine might be affected by the history of the flow field. Results show that, the existence of vortices at the initial state of the turbine, decreases the starting torque and leads to a lower initial acceleration of the turbine.
- At TSR<1.0, the main driving force of the turbine is the drag force, however, as the TSR grows, the lift force overweighs the drag force. The proposed method of the current study is able to accurately determine the instant of the minimum generated torque, which can be beneficial in selecting an appropriate strategy to enhance that critical torque.
- As the rotor TSR becomes greater than 1.0, the blade vortices shrink and the blades generate higher values of the lift force. As a result, the turbine acceleration increases considerably. However, at TSR>5, the blockage effect causes the turbine to act as a rigid cylinder and the air flows mainly around the turbine.
- It is shown in this paper that, the rotor inertia affects the turbine aerodynamic performance. As the rotor inertia increases, it takes a longer time for the turbine to reach its final velocity, in a manner that, the turbine might fail to reach the final condition and the rotation halts.
- Even at the final state, the turbine rotational velocity oscillates around a mean value and the amplitude of oscillations depends on the rotor moment of inertia. These oscillations affect the amplitude of the generated torque oscillations.
- As the rotor inertia decreases, the oscillations amplitude of the turbine rotational velocity increases. This can enable the turbine to pass higher resistant torques than those computed based on the traditional method.
- The numerical method proposed in this study, can be effectively employed to determine the importance of the rotor inertia on the start-up characteristics of the Darrieus-type wind turbines. Moreover, the effects of any external resistant torques, such as friction or generator torque, on the aerodynamic performance of the turbine can be determined.

Nomenclature

A	Turbine frontal area
a_f	Area vector
ATSR	Average Tip Speed Ratio
C_m	Torque coefficient
CFD	Computational Fluid Dynamics
C_p	Power coefficient
Div	Divergence operator
FSI	Fluid Structure Interaction
Grad	Gradient operator
I_{oz}	Rotor moment of inertia about the z-axis
I^*	Dimensionless moment of inertia
C_{Mr}	External resistant torque coefficient
M_τ	Moment due to the viscous forces
M	Total moments acting on the turbine
M_p	Moment due to the pressure forces
M_r	External resistant moments
p_f	Fluid pressure
R	Turbine radius
SST	Shear Stress Transition
S_φ	Source Term
V_∞	Air velocity
r_f	Distance vector from the body center of mass to the center of face f
T	Torque
TSR	Tip Speed Ratio
U	Time-averaged flow velocity vector
U_g	Grid velocity vector
URANS	Unsteady Reynolds Averaged Navier-Stokes
u, v	Fluid velocity components
VAWT	Vertical Axis Wind Turbine

Greek symbols

Γ	Diffusion coefficient
$\ddot{\theta}$	Rotor angular acceleration
ρ	Fluid density
τ_f	Shear stress
φ	A scalar quantity
ω	Rotor angular velocity

References

[1] M.M. Aslam Bhutta, N. Hayat, A.U. Farooq, Z. Ali, S.R. Jamil, Z. Hussain, Vertical axis wind turbine – a review of various configurations and design techniques, Renew. Sustain. Energy Rev. 16 (2012) 1926–1939.
[2] W. Tong, Wind Power Generation and Wind Turbine Design, Wit Press, 2010.
[3] I. Paraschivoiu, Wind Turbine Design: with Emphasis on Darrieus Concept, Presses inter Polytechnique, 2002.
[4] R.J. Templin, Aerodynamic Performance Theory for the NRC Vertical-axis Wind Turbine, National Research Council Canada, National Aeronautical Establishment, 1974.
[5] R.E. Wilson, P.B.S. Lissaman, S.N. Walker, Aerodynamic performance of wind turbines, energy research and development administration, Tech. Inf. Cent. (1976) 87–110.
[6] G. Bedon, M. Raciti Castelli, E. Benini, Optimization of a Darrieus vertical-axis wind turbine using blade element – momentum theory and evolutionary algorithm, Renew. Energy 59 (2013) 184–192.
[7] M. Islam, D.S.K. Ting, A. Fartaj, Aerodynamic models for Darrieus-type straight-bladed vertical axis wind turbines, Renew. Sustain. Energy Rev. 12 (2008) 1087–1109.
[8] A. Rossetti, G. Pavesi, Comparison of different numerical approaches to the study of the H-Darrieus turbines start-up, Renew. Energy 50 (2013) 7–19.
[9] M.H. Mohamed, Performance investigation of H-rotor Darrieus turbine with new airfoil shapes, Energy 47 (2012) 522–530.
[10] M.R. Castelli, E. Benini, Effect of blade inclination angle on a Darrieus wind turbine, J. Turbomach. 134 (2011), 031016–031016.
[11] L.-X. Zhang, Y.-B. Liang, X.-H. Liu, J. Guo, Effect of blade pitch angle on aerodynamic performance of straight-bladed vertical axis wind turbine, J. Cent. South Univ. 21 (2014) 1417–1427.
[12] T. Maître, E. Amet, C. Pellone, Modeling of the flow in a Darrieus water turbine: wall grid refinement analysis and comparison with experiments, Renew. Energy 51 (2013) 497–512.
[13] E. Amet, T. Maître, C. Pellone, J.L. Achard, 2D numerical simulations of blade-vortex interaction in a Darrieus turbine, J. Fluids Eng. 131 (2009), 111103–111103.
[14] V. D'Alessandro, S. Montelpare, R. Ricci, A. Secchiaroli, Unsteady Aerodynamics of a Savonius wind rotor: a new computational approach for the simulation of energy performance, Energy 35 (2010) 3349–3363.
[15] P. Jaohindy, H. Ennamiri, F. Garde, A. Bastide, Numerical investigation of airflow through a Savonius rotor, Wind Energy 17 (2014) 853–868.
[16] Y. Bazilevs, A. Korobenko, X. Deng, J. Yan, M. Kinzel, J.O. Dabiri, Fluid–structure interaction modeling of Vertical-Axis wind turbines, J. Appl. Mech. 81 (2014), 081006–081006.
[17] L.A. Danao, J. Edwards, O. Eboibi, R. Howell, A numerical investigation into the influence of unsteady wind on the performance and aerodynamics of a vertical axis wind turbine, Appl. Energy 116 (2014) 111–124.
[18] H. Niazmand, M. Anbarsooz, Slip flow over micron-sized spherical particles at intermediate Reynolds numbers, J. Mech. Sci. Technol. 26 (2012) 2741–2749.
[19] M. Anbarsooz, H. Niazmand, Heat transfer characteristics of slip flow over

solid spheres, proceedings of the institution of mechanical engineers, Part C J. Mech. Eng. Sci. 230 (19) (2015) 3431–3441, http://dx.doi.org/10.1177/0954406215612829.
[20] K.M. Almohammadi, D.B. Ingham, L. Ma, M. Pourkashan, Computational fluid dynamics (CFD) mesh independency techniques for a straight blade vertical axis wind turbine, Energy 58 (2013) 483–493.
[21] I. Dobrev, F. Massouh, CFD and PIV investigation of unsteady flow through Savonius wind turbine, Energy Proc. 6 (2011) 711–720.
[22] A. Inc., ANSYS FLUENT 12.0 Theory Guide, ANSYS, Inc., 2009.
[23] F.R. Menter, R.B. Langtry, S.R. Likki, Y.B. Suzen, P.G. Huang, S. Völker, A correlation-based transition model using local Variables—Part I: model formulation, J. Turbomach. 128 (2004) 413–422.
[24] R.B. Langtry, F.R. Menter, S.R. Likki, Y.B. Suzen, P.G. Huang, S. Völker, A correlation-based transition model using local Variables—Part II: test cases and industrial applications, J. Turbomach. 128 (2004) 423–434.
[25] A. Sagharichi, M.J. Maghrebi, A. ArabGolarcheh, Variable pitch blades: an approach for improving performance of Darrieus wind turbine, J. Renew. Sustain. Energy 8 (2016) 053305.
[26] M. Anbarsooz, Aerodynamic performance of helical Savonius wind rotors with 30° and 45° twist angles: experimental and numerical studies, proceedings of the institution of mechanical engineers, Part A J. Power Energy 230 (2016) 523–534.
[27] A. Kianifar, M. Anbarsooz, Blade curve influences on the performance of Savonius rotors: experimental and numerical, proceedings of the institution of mechanical engineers, Part A J. Power Energy 225 (2011) 343–350.
[28] D.O. Snyder, E.K. Koutsavdis, J.S.R. Anttonen, Transonic store separation using unstructured CFD with dynamic meshing, in: 33rd AIAA Fluid Dynamics Conference and Exhibit, Orlando, Florida, USA, 2003.
[29] ANSYS, Inc. ANSYS Manual, Release 15.0.
[30] J.H. Ferziger, M. Peric, Computational Methods for Fluid Dynamics, Springer, 2002.
[31] F. Trivellato, M. Raciti Castelli, On the Courant–Friedrichs–Lewy criterion of rotating grids in 2D vertical-axis wind turbine analysis, Renew. Energy 62 (2014) 53–62.
[32] M. Takao, H. Kuma, T. Maeda, Y. Kamada, M. Oki, A. Minoda, A straight-bladed vertical axis wind turbine with a directed guide vane row — effect of guide vane geometry on the performance, J. Therm. Sci. 18 (2009) 54–57.
[33] S.-C. Roh, S.-H. Kang, Effects of a blade profile, the Reynolds number, and the solidity on the performance of a straight bladed vertical axis wind turbine, J. Mech. Sci. Technol. 27 (2013) 3299–3307.
[34] R. Dominy, P. Lunt, A. Bickerdyke, J. Dominy, Self-starting capability of a Darrieus turbine, proceedings of the institution of mechanical engineers, Part A J. Power Energy 221 (2007) 111–120.
[35] N. Hill, R. Dominy, G. Ingram, J. Dominy, Darrieus turbines: the physics of self-starting, proceedings of the institution of mechanical engineers, Part A J. Power Energy 223 (2009) 21–29.
[36] E.N. Jacobs, K.E. Ward, R.M. Pinkerton, in: N.A.C.F. Aeronautics (Ed.), The Characteristics of 78 Related Airfoil Sections from Tests in the Variable-density Wind Tunnel, 1933.
[37] M. Zamani, M.J. Maghrebi, S.R. Varedi, Starting torque improvement using J-shaped straight-bladed Darrieus vertical axis wind turbine by means of numerical simulation, Renew. Energy 95 (2016) 109–126.
[38] M. Zamani, S. Nazari, S.A. Moshizi, M.J. Maghrebi, Three dimensional simulation of J-shaped Darrieus vertical axis wind turbine, Energy 116 (Part 1) (2016) 1243–1255.
[39] L.A. Danao, N. Qin, R. Howell, A numerical study of blade thickness and camber effects on vertical axis wind turbines, Proceedings of the Institution of Mechanical Engineers, Part: A J. Power Energy 226 (2012) 867–881.